JOURNAL OF THERMOPHYSICS AND HEAT TRANSFER
Vol. 8, No. 2, April–June 1994

Natural Convection of Micropolar Fluids in Concentric and Vertically Eccentric Annuli

J. S. Chiou* and Y. C. Chen†
National Cheng Kung University, Tainan, Taiwan 70101, Republic of China

Natural convection heat transfer of micropolar fluids bounded by two horizontal isothermal cylinders is numerically investigated for various Rayleigh number, radius ratio, and eccentricity. The governing equations, in terms of vorticity, stream function, and temperature, are expressed in a body-fitted coordinate system. The alternative direction implicit method and the successive overrelaxation technique are applied to solve the finite difference form of governing equations. Results indicate the heat transfer rate of a micropolar fluid is smaller than that of a Newtonian fluid, and the main controlling parameter is the dimensionless vortex viscosity. The eccentricity of an annulus heat exchanger may be caused by an imperfect installation. However, the allowance of having a positive eccentricity and enough radius ratio is indeed a benefit from heat transfer point of views.

Nomenclature

B = material parameter, L^2/j
e, E = dimensional and dimensionless eccentricities
f = dependent variable, defined in Eq. (27)
G = dimensionless angular velocity
g = gravity acceleration
J = Jacobian, $\partial(x, y)/\partial(\zeta, \eta)$
j = microinertia per unit mass
K = equivalent conductivity, $Nu/\overline{Nu}_c$
$\bar{K}$ = the mean equivalent conductivity
k_v = vortex viscosity
L = characteristic length, $r_o - r_i$
N = angular velocity
Nu_i, Nu_o = local Nusselt number for inner and outer cylinders
$\overline{Nu}$ = $\frac{1}{2}(\overline{Nu}_i + \overline{Nu}_o)$
$\overline{Nu}_c$ = mean Nusselt number of a concentric annulus when $Ra = 0$
$\overline{Nu}_s$ = mean Nusselt number of an eccentric annulus when $Ra = 0$
P, Q = coordinate control functions
Pr = Prandtl number, ν/α
R = radius ratio
Ra = Rayleigh number, $g\beta(T_h - T_c)L^3/\nu\alpha$
r_i, r_o = inner and outer radii
T, Θ = dimensional and dimensionless temperatures
t, τ = dimensional and dimensionless times
U, V = dimensionless of u, v
u, v = flow velocity in x and y directions
X, Y = dimensionless of x, y
x, y = Cartesian coordinates
α = thermal diffusivity
$\bar{\alpha}, \bar{\beta}, \bar{\gamma}$ = transformation factor defined in Eq. (17)
β = thermal expansion coefficient
Δ = material parameter, k_v/μ
θ = angle between the gravity force and the connection of annular axes
Λ = spin gradient viscosity
λ = material parameter, $\Lambda/j\mu$
ν, μ = kinematic and dynamic viscosities
ξ, η = body-fitted coordinates
ρ = density
ϕ, χ = coordinate control function defined in Eq. (18)
ψ, Ψ = dimensional and dimensionless stream functions
ω, Ω = dimensional and dimensionless vorticities

Received Oct. 12, 1992; revision received July 13, 1993; accepted for publication July 15, 1993.
*Associate Professor, Department of Mechanical Engineering.
†Graduate Student, Department of Mechanical Engineering.

Introduction

TO eliminate the human (operator's) error, a completely passive safety system is one of the major conceptual designs for a new-generation nuclear powerplant. The natural convection heat transfer of liquid metals in a confined enclosure is considered as an important problem to the passive cooling system. Usually, the liquid metals are considered as a Newtonian fluid, however, the ferro liquid or liquid with polymer additives are non-Newtonian. The local effects arising from microstructure and intrinsic motion of the fluid element will affect the flow motion and, in turn, alter the heat transfer characteristics.

Many researchers have investigated the natural convection of Newtonian fluid in a confined space. An excellent review was given by Ostrach.[1] Regarding the annular geometry, Kuehn and Goldstein[2,3] performed the experimental and theoretical study of natural convection in an annulus between horizontal cylinders. To facilitate the numerical calculation in dealing with the eccentric annulus, Prusa and Yao[4] used the radial coordinate transformation, while Cho et al.[5] applied the bipolar coordinate system to treat both eccentric and concentric annuli in a consistent way.

As far as micropolar fluid is concerned, the theory was, in sequence, developed by Eringen,[6–8] in which the local effect resulting from microstructure and gyration motions of the fluid elements were taken into consideration. The non-Newtonian behavior of liquid crystals, ferro liquids, and polymeric fluids were studied by many researchers, a detailed review made by Ariman et al.[9] demonstrated that for linear, viscous, and isotropic fluids, the non-Newtonian behavior of the above mentioned liquids can be modeled as micropolar fluid theory. The study investigating the effect of microstructure on the free convection heat transfer in enclosures is very few. Jena and Bhattacharyya[10] analyzed the effect of microstructure on the thermal convection in a rectangular box of fluid heated from below, they revealed that the dimensionless parameters of vortex viscosity and micropolar heat conduction are important to the onset of convection.

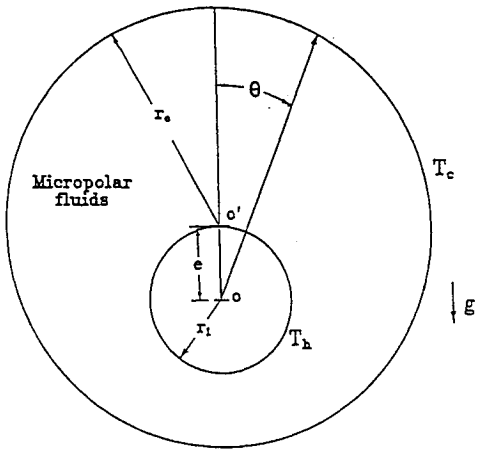

Fig. 1 Physical model.

In this study, the natural convection of micropolar fluid in concentric and vertically eccentric horizontal cylindrical annuli is analyzed. A finite difference solution is obtained for the governing equations in terms of stream function, vorticity, and temperature in a body-fitted coordinate system. The effect of aspect ratio, Rayleigh number, and eccentricity on the fluid flow and heat transfer characteristics are discussed.

Mathematical Formulation

Consider two horizontal cylinders of radii r_o and r_i located at $O'$and O, respectively, as shown in Fig. 1. The eccentricity of the inner cylinder is measured by the distance e. If inner cylinder is placed above the central position, e has a negative value, otherwise e is positive. For a natural convective heat transfer problem, the largest heat transfer variation due to eccentricity occurs when the direction of e is aligned with the gravitational direction. Therefore, this study focuses on the problems that e is vertically shifted.

The space between the inner and outer cylinders is filled by a kind of micropolar fluid. Initially, the annulus is at a uniform temperature T_c, and a quiescent state is assumed. At $t > 0$ the temperature of the inner cylinder is suddenly changed to a higher temperature T_h. To formulate the problem, we assumed that the fluid is incompressible, the friction heating is negligible, and the thermophysical properties of the fluid are constant, except the density, which follows the Boussinesq approximation. The governing equations for the two-dimensional problem fluid can be written as

Continuity

$$\omega = -\left(\frac{\partial^2\psi}{\partial x^2} + \frac{\partial^2\psi}{\partial y^2}\right) \tag{1}$$

Vorticity

$$\rho\left(\frac{\partial\omega}{\partial t} + u\frac{\partial\omega}{\partial x} + v\frac{\partial\omega}{\partial y}\right) = (\mu + k_v)\left(\frac{\partial^2\omega}{\partial x^2} + \frac{\partial^2\omega}{\partial y^2}\right) - k_v\left(\frac{\partial^2 N}{\partial x^2} + \frac{\partial^2 N}{\partial y^2}\right) + \rho g\beta\frac{\partial T}{\partial x} \tag{2}$$

Angular momentum

$$\rho j\left(\frac{\partial N}{\partial t} + u\frac{\partial N}{\partial x} + v\frac{\partial N}{\partial y}\right) = k_v(\omega - 2N) + \Lambda\left(\frac{\partial^2 N}{\partial x^2} + \frac{\partial^2 N}{\partial y^2}\right) \tag{3}$$

Energy

$$\frac{\partial T}{\partial t} + u\frac{\partial T}{\partial x} + v\frac{\partial T}{\partial y} + \alpha\left(\frac{\partial^2 T}{\partial x^2} + \frac{\partial^2 T}{\partial y^2}\right) \tag{4}$$

where ψ is stream function and N is the component of microrotation.

The initial conditions are

$$t < 0, \quad \psi = \omega = N = 0, \quad T = T_c$$

Since the geometry is symmetric to the vertical axis, the global flow circulation around the inner cylinder is assumed absent, the boundary conditions are expressed as

$$t \geq 0,\ r = r_i: \quad T = T_h, \quad \psi = 0, \quad \omega = -\nabla^2\psi, \quad N = \tfrac{1}{2}\omega$$

$$r = r_o: \quad T = T_c, \quad \psi = 0, \quad \omega = -\nabla^2\psi, \quad N = \tfrac{1}{2}\omega$$

Introduce the following dimensionless variables:

$$x = \frac{x}{L}, \quad y = \frac{y}{L}, \quad \Psi = \frac{\psi}{\alpha}, \quad \Omega = \frac{\omega L^2}{\alpha}$$

$$U = \frac{uL}{\alpha}, \quad V = \frac{vL}{\alpha}, \quad G = \frac{NL^2}{\alpha}, \quad \Theta = \frac{T - T_c}{T_h - T_c}$$

and $\tau = (t\alpha/L^2)$, where the characteristic length $L = r_o - r_i$, the governing equations in terms of the dimensionless variables are

$$\frac{\partial^2\Psi}{\partial x^2} + \frac{\partial^2\Psi}{\partial y^2} = -\Omega \tag{5}$$

$$\frac{\partial\Omega}{\partial\tau} + U\frac{\partial\Omega}{\partial X} + V\frac{\partial\Omega}{\partial Y} = Pr(1 + \Delta)\left(\frac{\partial^2\Omega}{\partial X^2} + \frac{\partial^2\Omega}{\partial Y^2}\right) - Pr\Delta\left(\frac{\partial^2 G}{\partial X^2} + \frac{\partial^2 G}{\partial Y^2}\right) + PrRa\frac{\partial\Theta}{\partial X} \tag{6}$$

$$\frac{\partial G}{\partial\tau} + U\frac{\partial G}{\partial X} + V\frac{\partial G}{\partial Y} = Pr\Delta B(\Omega - 2G) + Pr\lambda\left(\frac{\partial^2 G}{\partial X^2} + \frac{\partial^2 G}{\partial Y^2}\right) \tag{7}$$

$$\frac{\partial\Theta}{\partial\tau} + U\frac{\partial\Theta}{\partial X} + V\frac{\partial\Theta}{\partial Y} = \left(\frac{\partial^2\Theta}{\partial X^2} + \frac{\partial^2\Theta}{\partial Y^2}\right) \tag{8}$$

the initial and boundary conditions are

$$\tau < 0, \quad \Psi = \Omega = G = \Theta = 0 \tag{9}$$

when $\tau \geq 0$

$$\text{for } r = r_i: \quad \Theta = 1, \quad \Psi = 0, \quad \Omega = -\nabla^2\Psi, \quad G = \tfrac{1}{2}\Omega \tag{10}$$

$$\text{for } r = r_o: \quad \Theta = 0, \quad \Psi = 0, \quad \Omega = -\nabla^2\Psi, \quad G = \tfrac{1}{2}\Omega \tag{11}$$

In the above equations Δ, B, and λ are the dimensionless parameters defined as

$$\Delta = \frac{k_v}{\mu}, \quad B = \frac{L^2}{j}, \quad \lambda = \frac{\Lambda}{j\mu} \tag{12}$$

Numerical Procedure

To solve this problem, the governing equations as well as initial and boundary conditions in x, y are first transformed

in terms of ξ, η. The advantage of the body-fitted coordinates is that the complex physical domain is transformed into a rectangular computational domain where a regular mesh can be imposed (see Fig. 2). As discussed by Thomas and Middlecoff,[11] the rectangular mesh can be generated by solving a system of Poisson equations of the form

$$\xi_{xx} + \xi_{yy} = P(\xi, \eta) \tag{13}$$

$$\eta_{xx} + \eta_{yy} + Q(\xi, \eta) \tag{14}$$

Since it is desirable to perform all numerical computations in the transformed plane, the dependent and independent variables in Eqs. (13) and (14) must be interchanged to the forms of

$$\bar{\alpha}X_{\xi\xi} - 2\bar{\beta}X_{\xi\eta} + \bar{\gamma}X_{\eta\eta} + J^2(PX_\xi + QX_\eta) = 0 \tag{15}$$

$$\bar{\alpha}Y_{\xi\xi} - 2\bar{\beta}Y_{\xi\eta} + \bar{\gamma}Y_{\eta\eta} + J^2(PY_\xi + QY_\eta) = 0 \tag{16}$$

where $\bar{\alpha}$, $\bar{\beta}$, and $\bar{\gamma}$ are the transformation coefficients, and J is the Jacobian of the transformation given by

$$\begin{aligned} \bar{\alpha} &= X_\eta^2 + Y_\eta^2 \qquad \bar{\beta} = X_\xi X_\eta + Y_\xi Y_\eta \\ \bar{\gamma} &= X_\xi^2 + Y_\xi^2 \qquad J = X_\xi X_\eta - X_\eta Y_\xi \end{aligned} \tag{17}$$

The functions P and Q in Eqs. (15) and (16) are coordinate control functions that allow node points to be concentrated in certain desired regions. Here, we set

$$\begin{aligned} P &= \phi(\xi, \eta)(\xi_x^2 + \xi_y^2) \\ Q &= \chi(\xi, \eta)(\eta_x^2 + \eta_y^2) \end{aligned} \tag{18}$$

Substituting Eq. (18) into Eqs. (15) and (16), the functions $\phi(\xi, \eta)$ and $\chi(\xi, \eta)$ can be expressed as

$$\begin{aligned} \phi(\xi, \eta) &= -(X_\xi X_{\xi\xi} + Y_\xi Y_{\xi\xi})/(X_\xi^2 + Y_\xi^2) \qquad (\eta \text{ is const}) \\ \chi(\xi, \eta) &= -(X_\eta X_{\eta\eta} + Y_\eta Y_{\eta\eta})/(X_\eta^2 + Y_\eta^2) \qquad (\xi \text{ is const}) \end{aligned} \tag{19}$$

The elliptic Eqs. (15) and (16) are discretized by the finite difference method, and the resulting nonlinear algebraic equations are solved numerically by the SOR technique. The coefficients $\bar{\alpha}$, $\bar{\beta}$, $\bar{\gamma}$, and J are computed at each point and are stored for the numerical solutions of the governing equations as discussed below.

In terms of the transformed coordinates, the governing Eqs. (5–8) become

$$\begin{aligned} &(1/J^2)(\bar{\alpha}\Psi_{\xi\xi} - 2\bar{\beta}\Psi_{\xi\eta} + \bar{\gamma}\Psi_{\eta\eta}) \\ &\quad + P(\xi, \eta)\Psi_\xi + Q(\xi, \eta)\Psi_\eta = -\Omega \end{aligned} \tag{20}$$

$$\begin{aligned} &\Omega_\tau + (1/J)(\Psi_\eta\Omega_\xi - \Psi_\xi\Omega_\eta) = Pr(1 + \Delta)[(1/J^2)(\bar{\alpha}\Omega_{\xi\xi} \\ &\quad - 2\bar{\beta}\Omega_{\xi\eta} + \bar{\gamma}\Omega_{\eta\eta}) + P(\xi, \eta)\Omega_\xi + Q(\xi, \eta)\Omega_\eta] \\ &\quad - Pr\Delta[(1/J^2)(\bar{\alpha}G_{\xi\xi} - 2\bar{\beta}G_{\xi\eta} + \bar{\gamma}G_{\eta\eta}) + P(\xi, \eta)G_\xi \\ &\quad + Q(\xi, \eta)G_\eta] + (PrRa/J)(Y_\eta\Theta_\xi - Y_\xi\Theta_\eta) \end{aligned} \tag{21}$$

$$\begin{aligned} &G_\tau + (1/J)(\Psi_\eta G_\xi - \Psi_\xi G_\eta) = PrB\Delta(\Omega - 2G) \\ &\quad + Pr\lambda[(1/J^2)(\bar{\alpha}G_{\xi\xi} - 2\bar{\beta}G_{\xi\eta} + \bar{\gamma}G_{\eta\eta}) \\ &\quad + P(\xi, \eta)G_\xi + Q(\xi, \eta)G_\eta] \end{aligned} \tag{22}$$

$$\begin{aligned} &\Theta_\tau + (1/J)(\Psi_\eta\Theta_\xi - \Psi_\xi\Theta_\eta) = (1/J^2)(\bar{\alpha}\Theta_{\xi\xi} \\ &\quad - 2\bar{\beta}\Theta_{\xi\eta} + \bar{\gamma}\Theta_{\eta\eta}) + P(\xi, \eta)\Theta_\xi + Q(\xi, \eta)\Theta_\eta \end{aligned} \tag{23}$$

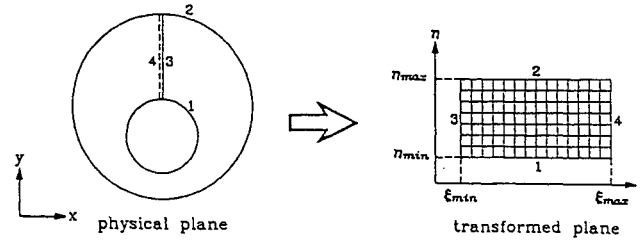

Fig. 2 Coordinate transformation.

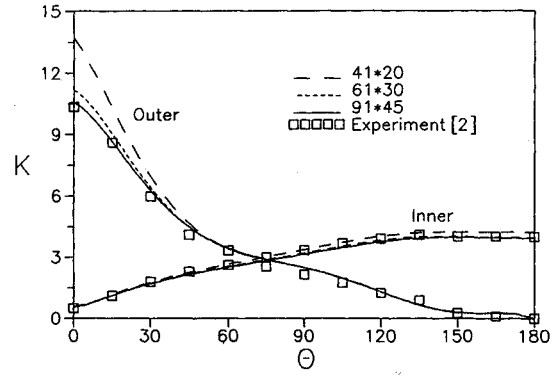

Fig. 3 Calculated equivalent conductivities at different grid nodings (Pr = 0.706, Ra = 5 × 10⁴, R = 2.6).

As a result of transformation the annulus is transformed into a rectangular domain (see Fig. 2), the corresponding initial and boundary conditions become

$$\tau < 0, \quad \Omega = \Psi = G = \Theta = 0 \tag{24}$$

$$\begin{aligned} &\tau \geq 0, \quad \eta = \eta_{\min}: \quad \Psi = 0, \quad \Theta = 1, \quad G = \tfrac{1}{2}\Omega \\ &\Omega = (-1/J^2)(\bar{\alpha}\Psi_{\xi\xi} - 2\bar{\beta}\Psi_{\xi\eta} + \bar{\gamma}\Psi_{\eta\eta}) - Q\Psi_\eta - P\Psi_\xi \end{aligned} \tag{25}$$

$$\begin{aligned} &\eta = \eta_{\max}: \quad \Psi = 0, \quad \Theta = 0, \quad G = \tfrac{1}{2}\Omega \\ &\Omega = (-1/J^2)(\bar{\alpha}\Psi_{\xi\xi} - 2\bar{\beta}\Psi_{\xi\eta} + \bar{\gamma}\Psi_{\eta\eta}) - Q\Psi_\eta - P\Psi_\xi \end{aligned} \tag{26}$$

In our program, $\eta_{\min}$ in Eq. (25) is set to be zero, and both $\Delta\eta$ and $\Delta\xi$ are set to be unity for simplicity purpose. The value of $\eta_{\max}$ in Eq. (26) is thus equal to the maximum node number minus one. For example, if the grid noding is 61 × 30, then $\eta_{\max}$ is 29 (=30 − 1). Equations (20–23) are discretized by the finite difference method with the time derivative terms approximated by forward differences and the spatial derivative terms approximated by central differences. The tracation errors have the order of $O(\Delta t)$ and $O(\Delta h)^2$, where Δt is the time step size and Δh is either $\Delta\eta$ or $\Delta\xi$. The finite difference equation for stream function, Eq. (20), was solved by the SOR method, while the finite difference forms of Eqs. (21–23) were solved by the ADI method. To see the effect of mesh size on the numerical results, computations for a concentric annulus were carried out using three different mesh sizes, the resulting equivalent conductivities are presented in Fig. 3. The mean equivalent conductivities obtained from three different mesh sizes are similar to each other, but the local value of outer cylinder at θ = 0 deg is sensitive to the noding size, and the result seems to converge at 91 × 45. In order to save the computation effort, the results presented in this article are all obtained by using the grid size of 61 × 30, and with a time increment of $\Delta t = 10^{-4}$ for $Ra \leq 2 \times 10^4$, and $\Delta t = 10^{-5}$ for $2 \times 10^4 < Ra \leq 5 \times 10^5$. The converge criterion of

$$\frac{\max|f_{i,j}^m - f_{i,j}^{m-1}|}{\max|f_{i,j}^m|} \leq 10^{-4} \tag{27}$$

was used, where f represents Θ, Ω, G, or Ψ, and m is the number of iterations.

After the convergence criteria were satisfied in each step, computations were also carried out for the local and mean Nusselt numbers at the inner and outer radii, which are defined as follows:

$$Nu_i = -\frac{\ell_a R}{2}\left(r\frac{\partial\Theta}{\partial r}\right)_{r=r_i} = -\frac{\ell_a R}{2}\left(\frac{\tilde{\gamma}\Theta_\eta - \tilde{\beta}\Theta_\xi}{J\sqrt{\tilde{\gamma}}}\right)_{\eta=\eta_{\min}} \tag{28a}$$

$$Nu_o = -\frac{\ell_a R}{2}\left(r\frac{\partial\Theta}{\partial r}\right)_{r=r_o} = -\frac{\ell_a R}{2}\left(\frac{\tilde{\gamma}\Theta_\eta - \tilde{\beta}\Theta_\xi}{J\sqrt{\tilde{\gamma}}}\right)_{\eta=\eta_{\max}} \tag{28b}$$

$$\overline{Nu}_i = \frac{1}{2\pi}\int_0^{2\pi} Nu_i \, d\theta \tag{29a}$$

$$\overline{Nu}_o = \frac{1}{2\pi}\int_0^{2\pi} Nu_o \, d\theta \tag{29b}$$

where $R = r_o/r_i$ (radius ratio).

Results and Discussion

The accuracy of numerical solution is verified by comparing the calculated results with the measured data and other calculated results. Figure 4 shows the streamlines and isotherms presented in van Dyke's book,[12] and the corresponding calculated results. Figure 5 shows the comparison between the calculated isotherms (on the left) and the measured isotherms (on the right) for air bounded by two horizontal (concentric and eccentric) cylinders. The measurements were performed by Kuehn and Goldstein.[2,3] Table 1 compares the calculated mean equivalent conductivities by the present study and by Kuehn and Goldstein[2] for a concentric annulus. The equivalent conductivity is defined as $\bar{K} = (\overline{Nu}/\overline{Nu}_c)$, where $\overline{Nu}_c$ is the value of $\overline{Nu}$ at $Ra = 0$, called pure-conduction heat transfer parameter. From the comparisons, it is found that the present calculations agree very well with the measurements.

The transient mean Nusselt number is plotted in Fig. 6. It is found that the time required to reach the steady state is shorter when Rayleigh number is larger because flow is moving faster. For most of the application, the settle time is usually less than a minute, therefore, the transient behavior is not discussed further in this study.

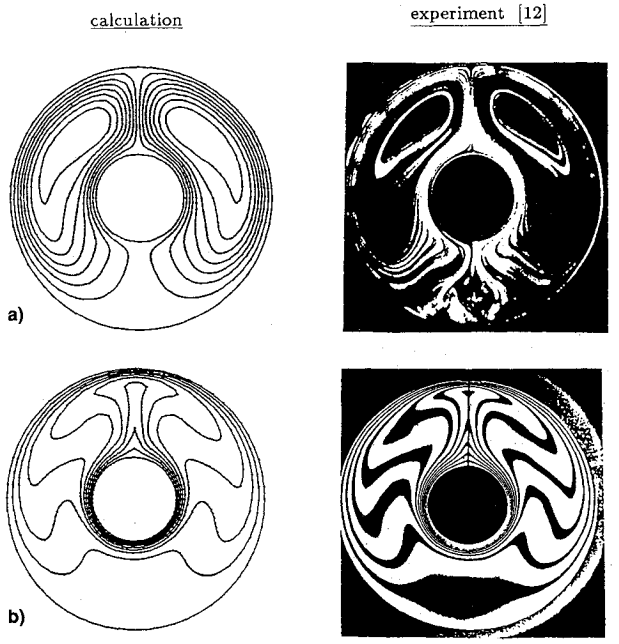

Fig. 4 Comparisons of: a) streamlines (Pr = 0.7, Gr = 1.2 × 10^5, R = 3) and b) isotherms (Pr = 0.7, Gr = 1.22 × 10^5, R = 3.14).

Table 1 Comparison of the calculated equivalent conductivity

			$\bar{K}$ (Present study)		$\bar{K}$ (Ref. 2)	
Ra	Pr	R	Inner	Outer	Inner	Outer
10^3	0.7	2.6	1.082	1.081	1.081	1.084
6 × 10^3	0.7	2.6	1.730	1.740	1.736	1.735
10^4	0.7	2.6	2.002	2.040	2.010	2.005
7 × 10^4	0.7	2.6	3.290	3.308	3.308	3.226

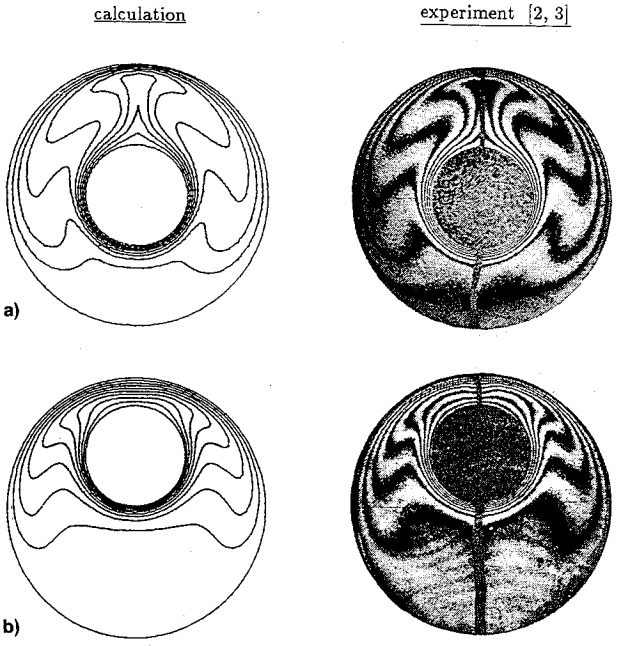

Fig. 5 Comparison of isotherms for a) concentric (E = 0.0) and b) eccentric annuli (E = −0.652) (Pr = 0.706, Ra = 4.8 × 10^4, R = 2.6).

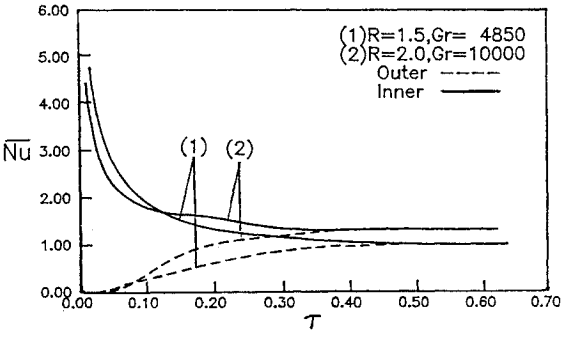

Fig. 6 Transient Nusselt number.

In the cases of micropolar fluid, the calculations were performed for the parameters of Δ = 0.5 and 1.0, λ = 0.5 and 1.5, the Prandtl number = 0.1, 0.7, and 10.0, R is from 1.2 to 5.0, and Gr ranges from 10^2 to 5 × 10^5. For the cases of eccentric annulus the dimensionless eccentricity, defined as $E = e/(r_o - r_i)$, covers from −1.0 to 1.0.

Figure 7 shows the calculated streamlines and isotherms for a concentric annulus at different Grashof numbers, for both Pr = 10 and Pr = 0.1. The cases with Pr = 10 simulate the lubricants containing suspended particles, and the other cases with Pr = 0.1 represent the ferro liquids with polymeric molecules. Because the problem is symmetric to the axis, each annulus contains only a half streamline on the left and a half isotherm on the right. Since the inner cylinder is kept hotter, the hot fluid near the inner cylinder rises upward due to thermal expansion. The uprising plume is then cooled down by the colder fluid near the upper part of outer cylinder. The

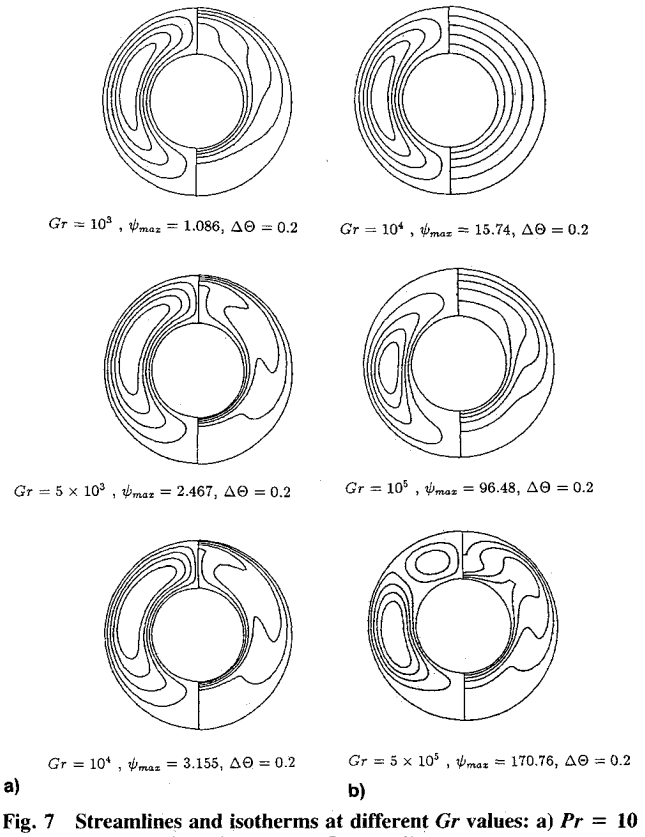

Fig. 7 Streamlines and isotherms at different *Gr* values: a) *Pr* = 10 and b) *Pr* = 0.1 (Δ = 0.5, λ = 0.5, *R* = 2).

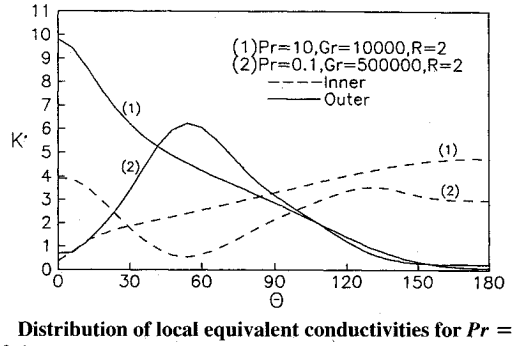

Fig. 8 Distribution of local equivalent conductivities for *Pr* = 10 and *Pr* = 0.1.

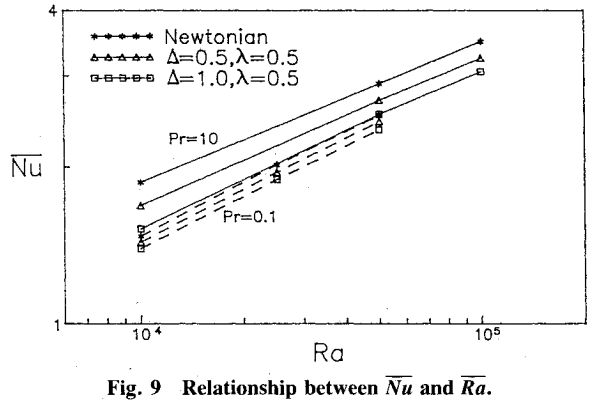

Fig. 9 Relationship between $\overline{Nu}$ and $\overline{Ra}$.

colder and denser fluid will eventually flow downward along the surface of outer cylinder. From Fig. 7 it is found that the maximum stream function increases with *Gr*. The basic flow pattern consists of one eddy, the center of this eddy (maximum stream function) tends to move up for *Pr* = 10 and move down for *Pr* = 0.1 as *Gr* increases. This behavior was also obtained by Custer et al.,[13] who used double perturbation expansions to solve the Newtonian flow in a concentric annulus. At the case of *Pr* = 0.1 and *Gr* = 5×10^5, a weak eddy besides the main eddy is also formed, this bicellular streamline also appeared in Ref. 13. As a result of the difference in streamlines and isotherms, the local *K* for *Pr* = 10 and *Pr* = 0.1 also behave different. Figure 8 depicts *K* vs θ for the case of *Pr* = 10, and the maximum *K* is located at θ = 0 deg for outer cylinder and θ = 180 deg for inner cylinder, which is similar to the case of air (*Pr* = 0.7). For the case of *Pr* = 0.1, the maximum *K* of outer cylinder and the minimum *K* of inner cylinder are located at θ = 60 deg, where the thermal boundary layer has the extreme value.

The increase of *R* has the same effect as the increase of *Gr* on the streamlines and isotherms (not shown here), however, the increase rate becomes insignificant once *R* > 2. This is because when *R* < 2 the flow circulation is restricted by the boundary wall, the heat transfer rate is mainly contributed

Table 2 Mean Nusselt number at different λ

Pr	*Gr*	λ	$\overline{Nu_i}$	$\overline{Nu_o}$
10	10^4	0.5	3.182	3.307
		1.5	3.184	3.370
0.1	2.5×10^5	0.5	1.941	1.969
		1.5	1.961	1.992

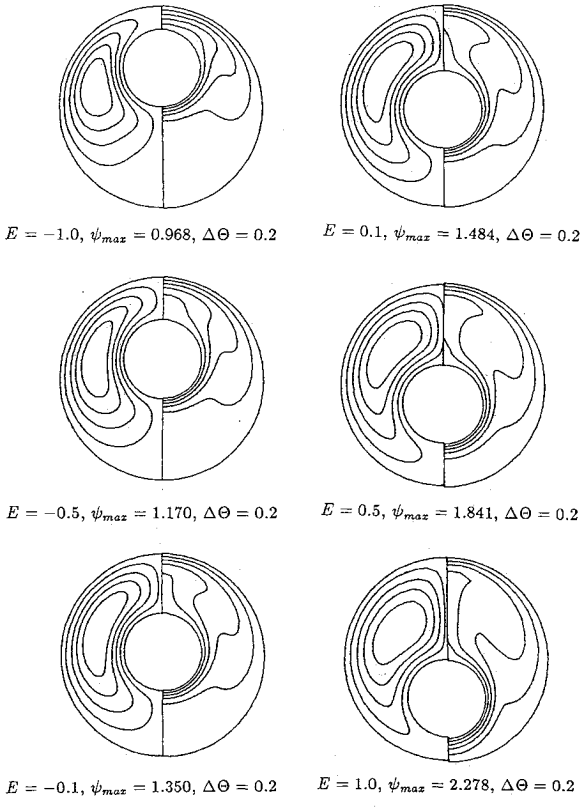

Fig. 10 Streamlines and isotherms at different eccentricities (*Pr* = 10, *Gr* = 2000, Δ = 0.5, λ = 0.5, *R* = 2.6).

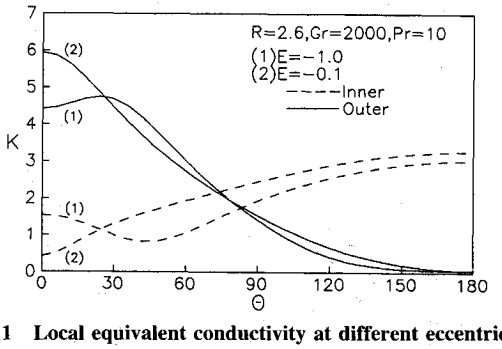

Fig. 11 Local equivalent conductivity at different eccentricities.

Table 3 K_c and $\bar{K}$ at different eccentricities ($R = 2.6$, $\Delta = 0.5$, $\lambda = 0.5$)

E	−1.0	−0.5	−0.1	0.1	0.5	1.0
K_c ($Ra = 0$)	1.302	1.060	1.001	1.001	1.060	1.302
$\bar{K}$ ($Pr = 10$, $Gr = 2000$)	1.971	2.053	2.210	2.267	2.352	2.530
$\bar{K}$ ($Pr = 0.1$, $Gr = 10^5$)	1.702	1.543	1.524	1.593	1.758	2.701

by conduction. As R increases, the flow circulation increases with the mean Nusselt number. After $R > 2$, the flow vortex can be freely formed in the annulus, the convective enhancement due to flow circulation becomes insignificant as long as Ra remained constant. The stream function (or flow velocity) will increase again once Ra increases. In fact, it is found from Fig. 9 that $\overline{Nu}$ is linearly increased with Ra in a log-log scale, which means the mean Nusselt number can be expressed as

$$\overline{Nu} = aRa^b$$

for both $Pr = 10$ and $Pr = 0.1$ where a, b are constants. Figure 9 also shows that the mean Nusselt number decreases when the vortex viscosity (Δ) increases. This is because the increase in vortex viscosity will reduce the stream function, i.e., slow down the flow velocity. On the other hand, the increase in spin gradient viscosity (λ) tends to impede the fluid particle spin (i.e., it will consume less energy in spinning) and accelerates the flow circulation, thus enhancing the heat transfer. However, the heat transfer enhancement due to the increase of λ is insignificant, because the effect of λ to the flow circulation is only a secondary factor. This can be found from the calculated results presented in Table 2, where the mean Nusselt number is found to increase slightly when λ increases from 0.5 to 1.5.

The calculations were also made for an eccentric annulus with the dimensionless eccentricity ranging from −1.0 to 1.0. Figure 10 shows the streamlines and isotherms for some selected eccentricities. As mentioned earlier, usually the maximum local heat transfer is located near $\theta = 0$ deg, where the heated uprising fluid begins to form the vortex. When the inner cylinder is moved downward (E is positive), more spaces near $\theta = 0$ deg are provided for flow to circulate. As a result, the stream function becomes larger (see Fig. 10) and the local heat transfer rate becomes higher. On the other hand, when the inner cylinder is moved upward (E is negative), the space near $\theta = 0$ deg becomes narrower. The narrow gap at $\theta = 0$ deg restricts flow circulation, and thus reduces stream function and heat transfer rate. The local maximum equivalent conductivity of $E = -1.0$ in Fig. 11 shifts from $\theta = 0$ deg to $\theta = 30$ deg, also indicating that the heat transfer rate near $\theta = 0$ deg is depressed because of poor circulation.

The values of specific conductivity K_c and $\bar{K}$ for different eccentricities are presented in Table 3. The definitions of K_c and $\bar{K}$ are $K_c = (Nu_s/Nu_c)$ and $\bar{K} = \frac{1}{2}(\overline{Nu}_o + \overline{Nu}_i)/Nu_c$. Since K_c stands for relative pure-conduction, its value is solely determined by the distance between the inner and outer cylinders. The value of K_c should be kept the same as long as R remained constant, and the value doesn't vary with the change of Pr. Table 3 shows the value of K_c is symmetric to the concentric position ($E = 0$), and increases as the degree of eccentricity increases. When Ra increases, the heat transfer rate due to convection effect gradually adds on. For the case of $Pr = 10$ and $Gr = 2 \times 10^3$, the heat transfer rate is dominated by convection effect. This can be found from Table 3, where $\bar{K}$ is minimum at $E = -1.0$ and maximum at $E = 1.0$ due to the effect of flow circulation. On the other hand, the conduction effect is very strong for the case of $Pr = 0.1$. Even at $Gr = 10^5$, the value of $\bar{K}$ at $E = -1.0$ is still larger than that at $E = -0.1$.

The maximum variation of mean equivalent conductivity due to eccentricity (compares to $\bar{K}$ at $E = 0$) is only moderate for the case of $Pr = 10$, but is much bigger for the case of $Pr = 0.1$. This is because the positive eccentricity cannot only promote the convection effect and also greatly enhance the conduction effect for the fluid with low Pr.

Concluding Remarks

Natural convection of micropolar fluid in both concentric and vertically eccentric annuli has been investigated numerically. From the calculated results, it is found that the mean Nusselt number increases with the flow's Rayleigh number and the ratio of outer radius to inner radius. The relation between the mean Nusselt number and the Rayleigh number can be expressed as $\overline{Nu} = aRa^b$ for $10^4 < Ra < 10^5$. Under the same Rayleigh number and radius ratio, the mean Nusselt number for micropolar fluid is lower than that for Newtonian fluid. This is because the micropolar fluid possesses vortex viscosity which will retard the vortex formation and slow down the flow circulation. The local equivalent conductivity can be greatly varied by the degree of eccentricity. This local effect is similar to the effect of radius ratio on the Nusselt number in a concentric annulus.

In terms of overall effect, the change of mean equivalent conductivity due to the degree of eccentricity is larger if the fluid has a low Prandtl number. The positive eccentricity can improve the mean equivalent conductivity, but the negative eccentricity may not be a detriment to the mean heat transfer rate if the Prandtl number of micropolar fluid is low.

References

[1]Ostrach, S., "Natural Convection in Enclosures," *Advances in Heat Transfer*, Vol. 8, 1972, pp. 161–227.

[2]Kuehn, T. H., and Goldstein, R. J., "An Experimental and Theoretical Study of Natural Convection in the Annulus Between Horizontal Concentric Cylinders," *Journal of Fluid Mechanics*, Vol. 24, Pt. 4, 1976, pp. 695–719.

[3]Kuehn, T. H., and Goldstein, R. J., "An Experimental Study of Natural Convection Heat Transfer in Concentric and Eccentric Horizontal Cylindrical Annuli," *Journal of Heat Transfer*, Vol. 100, Nov. 1978, pp. 635–640.

[4]Prusa, J., and Yao, L. S., "Natural Convection Heat Transfer Between Eccentric Horizontal Cylinders," *Journal of Heat Transfer*, Vol. 105, Feb. 1983, pp. 108–116.

[5]Cho, C. H., Chang, K. S., and Park, K. H., "Numerical Simulation of Natural Convection in Concentric and Eccentric Horizontal Cylindrical Annuli," *Journal of Heat Transfer*, Vol. 104, Nov. 1982, pp. 624–630.

[6]Eringen, A. C., "Simple Microfluids," *International Journal of Engineering Science*, Vol. 2, No. 2, 1964, pp. 205–217.

[7]Eringen, A. C., "Theory of Micropolar Fluids," *Journal of Mathematical Mechanics*, Vol. 16, No. 1, 1966, pp. 1–18.

[8]Eringen, A. C., "Theory of Thermomicrofluids," *Journal of Mathematical Analysis and Applications*, Vol. 38, No. 2, 1972, pp. 480–495.

[9]Ariman, T., Turk, M. A., and Sylvester, N. D., "Microcontinuum Fluid Mechanics—A Review," *International Journal of Engineering Science*, Vol. 11, No. 8, 1973, pp. 905–930.

[10]Jena, S. K., and Bhattacharyya, S. P., "The Effect of Microstructure on the Thermal Convection in a Rectangular Box of Fluid Heated from Below," *International Journal of Engineering Science*, Vol. 24, No. 1, 1986, pp. 69–78.

[11]Thomas, P. D., and Middlecoff, J. F., "Direct Control of the Grid Point Distribution in Meshes Generated by Elliptic Equations," *AIAA Journal*, Vol. 18, No. 6, 1980, pp. 652–656.

[12]Van Dyke, M., "An Album of Fluid Motion," The Parabolic Press, Stanford, CA, 1982.

[13]Custer, J. R., and Shaughnessy, E. J., "Thermoconvective Motion of Low Prandtl Number Fluids Within a Horizontal Cylindrical Annulus," *Journal of Heat Transfer*, Vol. 99, Nov. 1977, pp. 596–602.